IEEE Access
Multidisciplinary | Rapid Review | Open Access Journal

Received 12 May 2023, accepted 5 July 2023, date of publication 10 July 2023, date of current version 18 July 2023.

Digital Object Identifier 10.1109/ACCESS.2023.3293655

RESEARCH ARTICLE

Dual-Band, Aperture-Shared Transmitarray for Vehicular SatCom Applications

REDA MADI[1], ANTONIO CLEMENTE[1], (Senior Member, IEEE), AND RONAN SAULEAU[2], (Fellow, IEEE)

[1]CEA, Leti, University of Grenoble Alpes, 38000 Grenoble, France
[2]CNRS, Institut d'Electronique et des Technologies du numéRique (IETR), UMR 6164, University of Rennes, 35000 Rennes, France

Corresponding author: Antonio Clemente (antonio.clemente@cea.fr)

This work was supported in part by the National Research Agency (ANR) through the Project ANR-ASTRID ArtiKa under Grant ANR-20-ASTR-0014-01.

ABSTRACT This paper proposes a novel design and the experimental characterization of a dual-band, shared aperture transmitarray operating in dual linear polarization at K/Ka-band. It is based on a 1-bit unit-cell realized using five metal layers and demonstrating low transmission loss (<2 dB). By combining the polarization rotation method and the stacked patch architecture, the proposed shared aperture transmitarray is able to shape the beam independently in both K- and Ka-bands. A 40 × 40-element prototype has been optimized by using an *ad-hoc* numerical tool and fabricated. The experimental results are in excellent agreement with the numerical and full-wave electromagnetic simulations. This flat lens is illuminated by two standard gain horns with a nominal gain of 10 dBi. They are mounted in orthogonal polarization and located at the same distance from the aperture (110 mm). A peak gain of 27.1 and 29.9 dBi has been achieved, respectively, at 18.7 and 28.5 GHz corresponding to an aperture efficiency of 26.1 and 22.3%. The possibility to steer mechanically the radiation pattern has also been experimentally proven. The proposed antenna system is a low-cost and compact solution for future vehicular broadband SatCom applications.

INDEX TERMS Transmitarray antenna, SatCom, SOTM, dual-band, dual-polarization, polarization manipulation.

I. INTRODUCTION

SATCOM-on-the-move applications (SOTM) on different mobile platforms will play a fundamental role in the future ''New Space'' era, also indicated as Internet-of-Space (IoS). Both the use of Low Earth Orbit (LEO) satellite technologies and the millimeter wave spectrum, such as the K/Ka-band, will enable the development of new SatCom broadband systems and services [1], [2], [3]. In this context, one of the key enablers for the integration of the future SOTM systems in relatively compact terrestrial platforms, such as in the case of vehicles, is the miniaturization of the antenna systems (see Fig. 1). In fact, highly efficient and directive antenna, with relative large radiating aperture, are used to compensate the signal fading at millimeter waves. Today several commercial antenna solutions have been developed for SOTM [3]; however, both aperture dimensions and costs are extremely large to allow their integration on the vehicle and meet the stringent requirements of the automotive market.

In addition to the high-gain, wideband and beam-steering specifications, SOTM communications at K/Ka-bands require innovative antenna solutions operating in full-duplex and dual polarization. Orthogonal polarization is required between up-link (27.5-31.0 GHz) and down-link (17.3-21.2 GHz) frequency ranges to improve the *Tx/Rx* isolation. Mechanical or electronic beam scanning is used at the terminal to guarantee a reliable communication link with one or more moving satellites. Flat mechanical solutions are typically based on continuous transverse stub (CTS) [4], [5] or Risley-prism antennas [6], [7], [8]. On the other hand, phased-array antennas with integrated circuits (IC) are very flexible architectures to electronically steer the radiated beam [9], [10].

The associate editor coordinating the review of this manuscript and approving it for publication was Raghvendra Kumar Chaudhary.

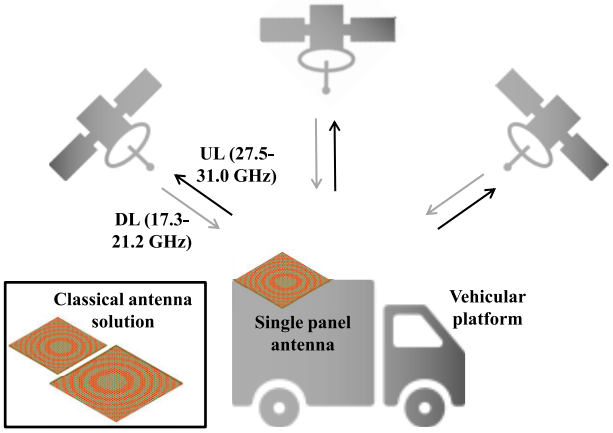

FIGURE 1. SatCom vehicular communication scenario at K-/Ka-band using a single panel antenna with mechanical steering.

An alternative and very promising solution for SatCom applications is based on transmitarray antennas [11]. A transmitarray is a spatially-fed architecture composed of a focal source/array and a flat panel composed of several hundred or thousands of unit-cells. The spherical electromagnetic wavefront radiated by the focal system and impinging on the transmitarray aperture is locally compensated in phase by the unit-cells and collimated in a specific direction of the far field. Varactors [12], RF-MEMS switches [13], or p-i-n diodes [14], [15], [16] can be integrated into the radiating aperture to electronically control the transmission phase of the unit-cells and dynamically steer/shape the antenna beam. Two separate panels are typically used at K/Ka-band to facilitate the implementation of full-duplex SatCom antenna systems. This leads to large antenna footprints that might be challenging to accommodate on moving platforms of limited size. Therefore aperture-shared solutions are attractive to overcome this major limitation. As presented in Fig. 1, a single-panel transmitarray antenna with mechanical beam-scanning is proposed in this paper for vehicular SOTM applications.

In this context dual-band, shared aperture transmitarrays with fixed beam or mechanical steering have been demonstrated in the last years at Ku- [17], [18], [19], [20], [21] and K/Ka-bands [22], [23], [24], [25], [26]. They are based predominantly on interleaved unit-cells with a lattice periodicity larger than half a wavelength. Such a lattice size induces the appearance of grating lobes in the visible range while scanning the antenna beam over a wide field of view. Interleaved technology represents an excellent solution with an aperture efficiency up to 53.0% [18] at Ku-band, where the ratio between the frequency bands is more favorable than in the K/Ka-bands. On the other side, stacked architectures [22], [26] allow us to reduce significantly the lattice size, but at the cost of a complex multilayer stack-up with a large number of dielectric and metal layers.

To circumvent these two limitations (compact lattice size and extremely complex multilayer architecture if compared to stacked architectures [22]) and obtain a relative 3-dB gain

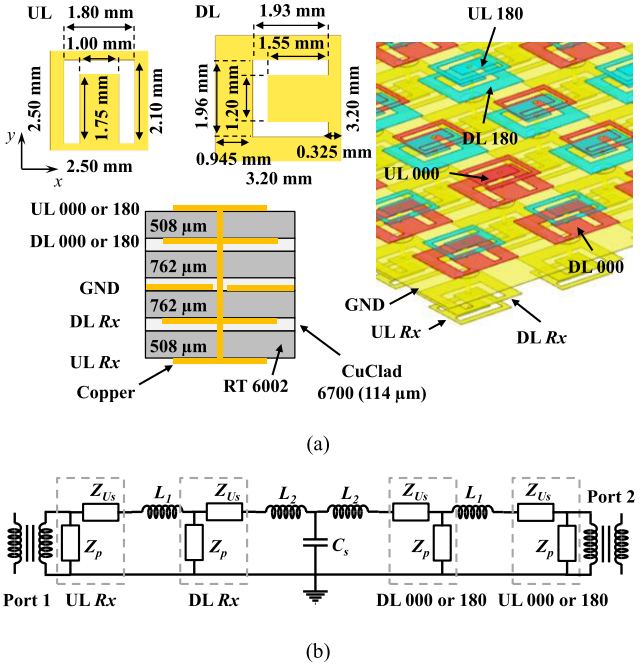

FIGURE 2. (a) Geometrical parameters of the U-slotted patch antennas, unit-cell stack-up, and schematic view of the proposed aperture-shared transmitarray. The red and blue patches indicated 000 or 180 unit-cells, respectively. (b) Equivalent Lumped element circuit of the stacked UC.

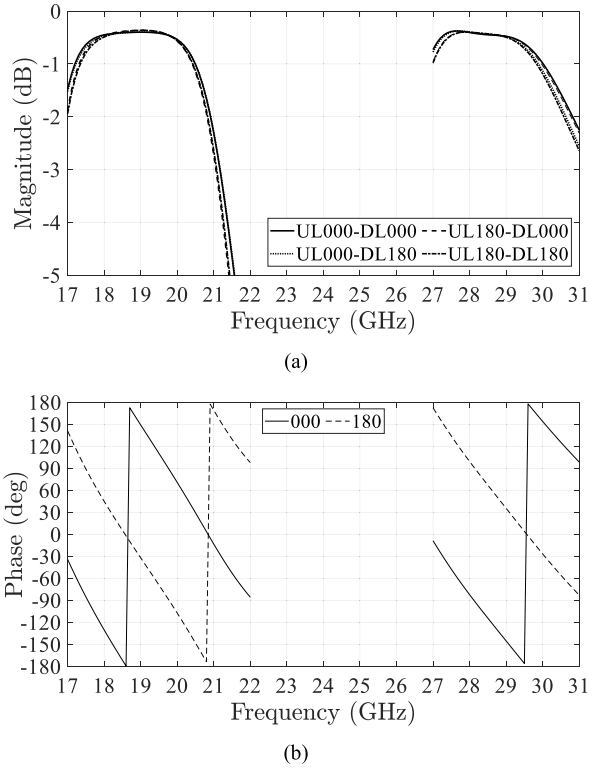

FIGURE 3. Simulated transmission coefficients of the dual-band, dual linearly-polarized UC as a function of frequency: magnitude of the cross-polar components.

bandwidth > 10% in each band, we introduce here a new dual-band, dual-linearly polarized unit-cell for transmitarray

at K/Ka-band (the center frequencies in the down- and up-link bands are 19 and 29 GHz respectively). This unit-cell is based on a stacked approach with five metal layers (see Fig. 1(a)). U-slotted patch antennas have been selected as radiating elements to obtain a wideband design [27]. The potentiality of this unit-cell has been discussed in our preliminary conference paper and compared to interleaved strategies [28]. Furthermore, the work proposed here drastically differs from [19], where U-slotted patch antennas are interleaved to design a single linearly-polarized transmitarray operating in dual-band at 12 and 14 GHz. It may appear at first thought that the proposed stacked unit-cell is not fundamentally different from the latter, but the different ratio between the frequency bands addressed in this paper makes our design more advanced. In fact, the stacked architecture is extremely sensitive to mutual coupling between radiating elements operating at different frequencies. Furthermore, the major limitation of the strategy proposed in [19] is the demonstrated gain bandwidth, which is lower than 8%.

The rest of this article is organized as follows. The geometry and operating principle of the proposed unit-cell are discussed in Section II. A design example is provided in Section III together with numerical and experimental results. Mechanical beam-steering is achieved by changing the relative position of the flat lens with respect to the center of the focal system. Finally, conclusions are drawn in Section IV.

II. DUAL-BAND DUAL-POLARIZED UNIT-CELL

As introduced in Section I, one of the keys to the integration on vehicles of high-gain antennas for Ka-satellite connectivity is the reduction of the radiating surface. To this end, we propose here a dual-band (K/Ka), dual linearly polarized unit-cell based on a stacked architecture. In SOTM applications at Ka-band, the targeted frequency bands are defined as 17.3-21.2 GHz and 27.5-31.5 GHz for the down-link and up-link, respectively. The use of the stacked approach leads to a much more compact lattice size if compared to the interleaving technique [23], [24], e.g. periodicity lower than half of a wavelength on the two bands. Furthermore, the compact lattice allows for a mitigation of the grating lobe phenomena in the visible region and an improved steering capability, as demonstrated in our preliminary conference paper [28]. This characteristic is also confirmed here in the case where the beam is steered mechanically.

A. ARCHITECTURE AND OPERATION PRINCIPLE

The geometry and physical dimensions of the proposed stacked unit-cell (UC) is represented in Fig. 2(a). Its lattice size is equal to 5×5 mm^2, which is equivalent to $0.48\lambda_{ul} \times 0.48\lambda_{ul}$ and $0.31\lambda_{dl} \times 0.31\lambda_{dl}$, where λ_{dl} and λ_{ul} indicate the wavelength in free space at 19 and 29 GHz respectively (DL and UL stand for down-link and up-link, respectively). To achieve a dual-band behavior, this UC includes four patch antennas loaded by U-shaped slots. Two patches are used for the receiving layer (Rx), and two patches for the transmitting one (Tx). The inner metal layers operate in the DL band and are printed on two 762-μm-thick substrates (Roger RT/Duroid 6002 substrates $\varepsilon_r = 2.94$, $\tan\delta = 0.0012$); they are linearly-polarized along x-axis. The outer metal layers correspond to the patches resonating at UL; they are printed on two 508-μm-thick substrates and are polarized along y-axis. The four substrates are bounded using three films of glue (Arlon CuClad 6700 films $\varepsilon_r = 2.35$, $\tan\delta = 0.0025$, thickness: 114 μm). A metalized via-hole located at the center of the rectangular radiating element (diameter: 200 μm) is used to connect the four patches and correctly feed the radiating elements. Finally, a circular slot (diameter: 1 mm) is etched in the ground plane to isolate this via (Fig. 2(a)).

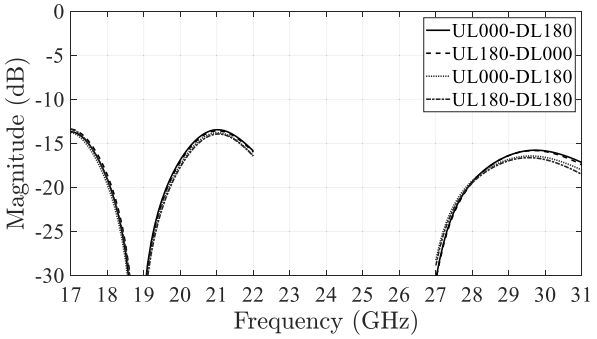

FIGURE 4. Simulated transmission coefficients of the dual-band, dual linearly-polarized UC as a function of frequency: magnitude of the cross-polar components.

In the proposed structure, both operation in dual-linear polarization and frequency isolation are achieved by imposing a 90° geometrical rotation between the UL and DL patch antennas of each unit-cell phase state. Moreover, the 1-bit of phase resolution is obtained independently in each band by rotating the Tx patches at UL or DL by 180° around the central metalized via, as indicated in Fig. 2(a). Both patch configurations in each band are labeled UL000 or DL000 and UL180 or DL180, respectively. Considering the different combinations of the four Tx patches (i.e. stacking UL000 with DL000, UL000 with DL180, UL180 with DL000, or UL180 with DL180), four phase-shift structures with 1-bit of phase resolution can be implemented to control independently the UL and DL phase distributions. Furthermore, the isolation between UL and DL has been improved by introducing a dissymmetry in the U-slot position of the patches operating at DL (e.g. a shift of 0.325 mm and 0.945 mm from the right- and left-edges of the patch, respectively in Fig. 2(a)). While, the U-slot of the UL patch is located at the center of the square patch antenna.

It is well known from the literature that a U-slot loaded patch antenna exhibit a dual resonance behavior [29], e.g. one resonance is due to the patch antenna (cavity mode TM_{10}) and the second one is generated by the U-slot. Combining these two resonances allows achieving a wideband radiating element. Their approximate expressions have been used in our previous work [30] to derive an equivalent model based on lumped elements. Considering the geometrical parameters of the four U-slotted patches, it is possible to represent each

patch as a series combination of a parallel RLC resonator (rectangular microstrip patch) and a complex impedance modelling the U-slot. These two resonators are indicated in Fig. 2(b) with the impedance terms $Z_p$and Z_{Us}, respectively. Furthermore, the metallized via in each of the dielectric layer can be modelled as an inductor L. Its value (L_1 or L_2) depends on the thickness and dielectric properties of the substrate. The hole in the ground plane is equivalent to a capacitor C. Finally, both patches are coupled to input/output 377 Ω free-space ports through ideal transformers. The different Lumped elements can be extracted analytically by considering the formulas presented in [30].

B. FREQUENCY RESPONSE

The proposed UC has been simulated using the full-wave electromagnetic software Ansys HFSS with periodic boundary conditions and Floquet ports. The simulated magnitude and phase of the transmission coefficients of the UC illuminated under normal incidence are plotted respectively in Fig. 3(a) and Fig. 3(b) for both phase states and each frequency band. The results under oblique incidence up to 45° are not given here for brevity purposes; as expected and as demonstrated previously in the case of U-slotted patch-based unit-cells [14], a negligible variation in amplitude and phase is observed when compared to normal incidence behavior.

The 1-dB transmission bandwidth of the UC reaches 17.4% and 10.7% at 19.5 GHz and 29 GHz, respectively with a minimum insertion loss lower than 0.5 dB. Furthermore, the 1-bit phase resolution is obtained over both entire frequency bands of interest. To study the isolation between DL and UL frequency bands, the four UC combinations have been analyzed in simulation as a function of the UC phase states; they are named UL000-DL000, UL180-DL000, UL000-DL180, and UL180-DL180. The numerical results are plotted in Fig. 3(b). They clearly show that thanks to the 90° rotation between UL and DL patches, a very similar frequency response is obtained for each UC combination. In the same way, no difference in the transmission phase response has been obtained for the same configurations. Furthermore, thanks to the 90° geometrical rotation of the UL and DL patch antennas, the simulated isolation between the two polarizations is lower than 13 and 16 dB on DL and UL frequency bands, respectively (see Fig. 4 for details). The cross-polarization component has been extracted by the full-wave simulation under normal incidence and considering the excitation of the fundamental mode for each frequency band on the *Rx* side of the unit-cell. Additional details on the UC geometry and surface current distributions are included in our preliminary work [25].

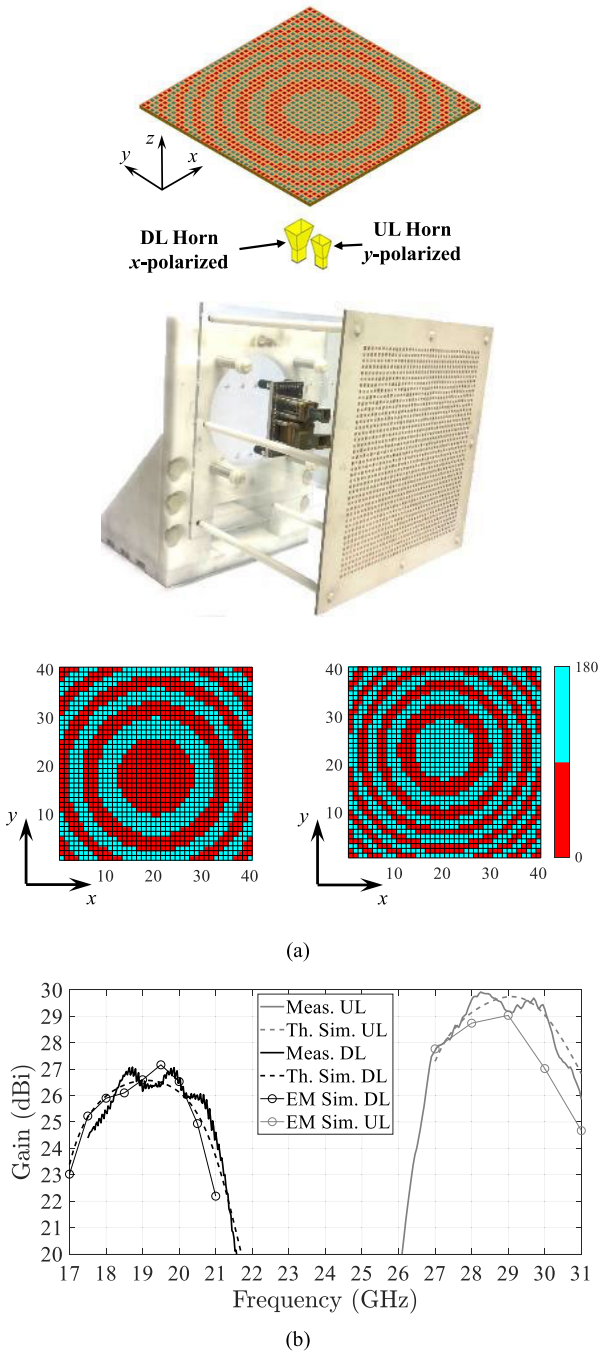

FIGURE 5. Measured 40 × 40-element transmitarray. (a) schematic view (top) and photograph (middle) of the antenna prototype with the optimized 1-bit phase gradients (DL left-bottom and UL right-bottom). In the picture, at each frequency band, red and blue pixels indicated a phase state 000 or 180, respectively. (b) frequency response at the downlink (DL) and uplink (UL) bands.

III. DUAL-BAND DUAL-POLARIZED TRANSMITARRAY

The schematic view of the 40 × 40-element transmitarray is presented in Fig. 5(a). The aperture has a surface equal to $200\times200\,\text{mm}^2$. Two pyramidal horn antennas (one for the DL and one for the UL frequency bands) are used to illuminate the TA panel. Their nominal gains are around 10 dBi. They are linearly-polarized along the *x*- and *y*-axes for the DL and UL frequency bands, respectively to guarantee a suitable excitation of the UC. Although both horns operate in different frequency bands, they are placed in the same focal plane to ease the antenna assembly and avoid shadowing effects and spurious scattering phenomena.

The focal distance F has been optimized using our *ad-hoc* numerical tool to find the best trade-off between illumination

TABLE 1. Performance comparison with existing dual-band, dual-polarized transmitarrays at K/Ka-BAnd.

		[22]	[23]	[24]	[26]	This work
Topology		Stacked	Interleaved	Interleaved	Stacked	Stacked
No. dielectrics		6	2	3	8	4
Phase resol.		Continuous	1-bit	Continuous	2-bits	1-bit
No. metal layers		7	3	3	13	5
Vias		No	Yes	No	Yes	Yes
Polarization		Single-LP	Dual-LP	Dual-CP*	Dual-CP	Dual-LP
***F/D* ratio**		~0.80	0.60	0.69	0.70	0.56
Lattice size (λ)	DL	0.23	0.40	0.35	0.35	0.33
	UL	0.35	0.60	0.53	0.53	0.50
Gain (dBi)	DL	24.6	27.4	15.3	26.8	27.1
	UL	27.2	28.4	15.3	28.2	29.9
3-dB BW (%)	DL	-	10.7	10.0	> 11.7	19.8
	UL	-	11.4	7.00	> 10.2	12.0
Ap. Eff. (%)	DL	36.0	20.1	10.0	24.6	26.1
	UL	29.0	21.2	6.00	15.6	22.3

*Circular polarization (CP). Linear polarization (LP)

taper and spill-over in both bands [31], [32]. The optimal value of F for DL and UL is 110 mm (corresponding to a F/D ratio equal to 0.56, where D is the aperture size). The UL and DL horns are shifted from the center respectively by ± 15 mm in the xy-plane. Even in this case, this position has been optimized to maximize the aperture efficiency and minimize the beam squint effects, when mechanical scanning is considered. These choices lead to an illumination level lower than -10 dB at the transmitarray aperture in both bands.

The optimized and fabricated prototype, including the UL and DL 1-bit phase gradients, is presented in Fig. 5(a). For each frequency band, these phase distributions are synthesized to collimate the beam at the broadside direction. The full-wave results of the focal sources and the active radiation patterns and scattering matrix of the UC, under normal incidence conditions, are taken into account in the optimization process. The required 1-bit phase gradient $\varphi_{UC}^{m}\left(S_{21}^{m}, f_{DL}, f_{UL}\right)$ is defined for each of the 1600 unit-cells using the expression in (1), as shown at the bottom of the page.

For a future integration of the proposed antenna system, to reduce the thickness of the antenna, the dual-horn system could be replaced by a dual-band, dual-polarized flat array generating a similar aperture taper than the one obtained with the actual illumination system. By slightly optimizing the phase gradients, an improvement of the gain could be also achieved thanks to the possibility to locate the flat array at the center of the focal plane. Dual-band folded architectures have been also preliminary investigated in the literature [33]. In this paper, the dual-horn focal structure has been selected to study and demonstrate the beam-steering capability of the antenna, which is an important feature in the case of vehicular SOTM applications.

A. PERFORMANCE AT BROADSIDE

The proposed TA behavior has been also studied using full wave simulations (Ansys HFSS version 2020.R1) to validate the numerical results obtained with our *ad-hoc* numerical tool [31], [32]. The finite element-boundary integral (FE-BI) solver has been employed to speed-up the simulation convergence and reduce the required computing resources. The simulation has been carried out using parallel computing (up to 8 cores) and 256 Gbits of RAM. The simulated peak gain (EM Sim.) is plotted in Fig. 5(b) as a function of frequency and is compared with the results achieved with the array-theory-based *ad-hoc* tool (Th. Sim.). The agreement

$$\varphi_{UC}^{m}\left(S_{21}^{m}, f_{DL}, f_{UL}\right) = \begin{cases} DL000 - UL000 & \text{if} -90^{\circ} \le \varphi_{UC}^{m}\left(S_{21}^{m}, f_{DL}, f_{UL}\right) < 90^{\circ} \\ DL000 - UL180 & \text{if} -90^{\circ} \le \varphi_{UC}^{m}\left(S_{21}^{m}, f_{DL}\right) < 90^{\circ} \wedge \left(\varphi_{UC}^{m}\left(S_{21}^{m}, f_{UL}\right) < -90^{\circ} \vee \varphi_{UC}^{m}\left(S_{21}^{m}, f_{UL}\right) \ge 90^{\circ}\right) \\ DL180 - UL000 & \text{if} \left(\varphi_{UC}^{m}\left(S_{21}^{m}, f_{DL}\right) < -90^{\circ} \vee \varphi_{UC}^{m}\left(S_{21}^{m}, f_{DL}\right) \ge 90^{\circ}\right) \wedge -90^{\circ} \le \varphi_{UC}^{m}\left(S_{21}^{m}, f_{UL}\right) \\ DL180 - UL180 & otherwise \end{cases} \quad (1)$$

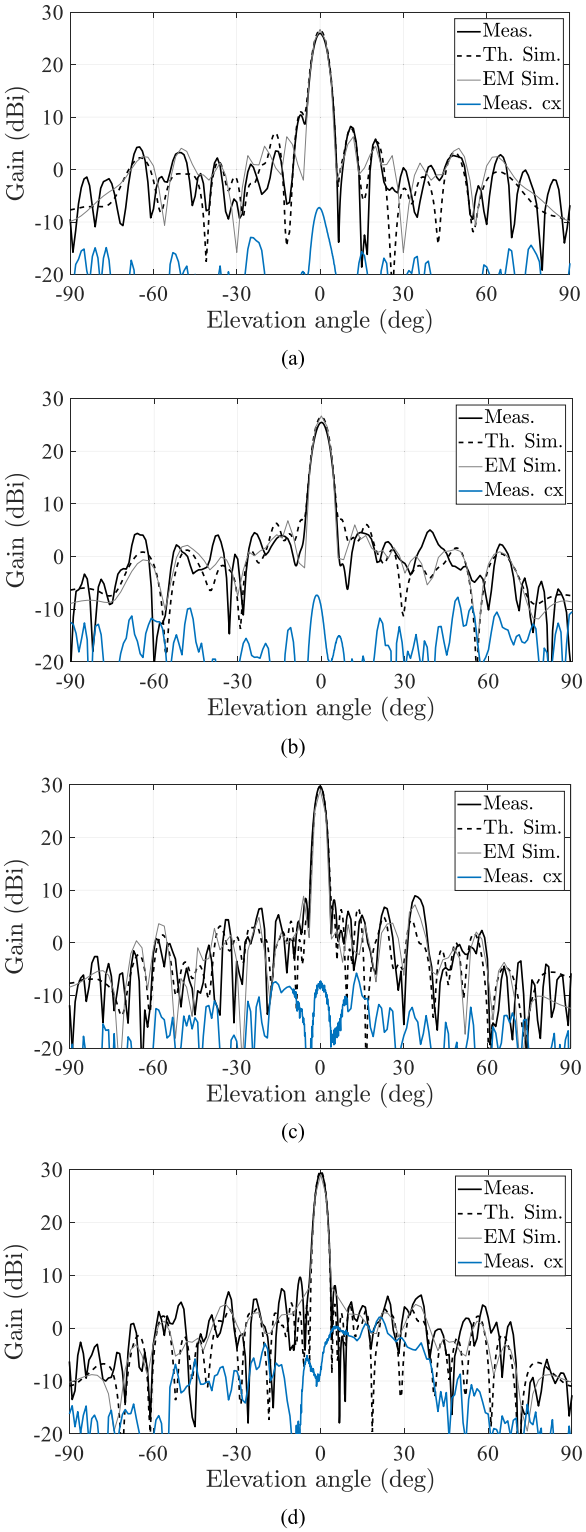

FIGURE 6. Measured, theoretical, and simulated gain radiation patterns at broadside. 19 GHz for the (a) E- and (b) H-planes, and 29 GHz for the (c) E- and (d) H-planes. Measured cross-polarization components are also reported (blue lines).

between both approaches is very satisfactory. The average error between both simulation methods is lower than 0.5 and 1 dB, respectively, in the DL and UL frequency bands. The

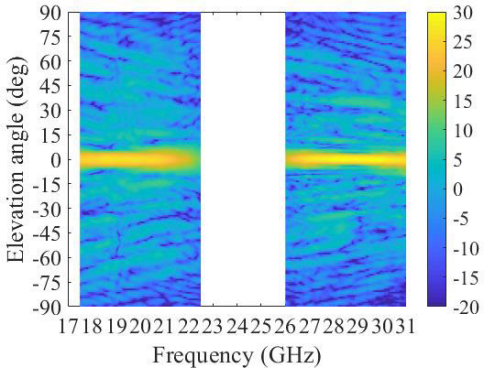

FIGURE 7. Measured gain radiation patterns at broadside. 2D pattern as a function of frequency.

slight discrepancy observed in the UL band is probably due to the imposed convergence criteria.

The antenna prototype has been fabricated using a standard PCB (Printed Circuit Board) process, with a copper thickness of 18 μm and a minimum line resolution of 200 μm $\pm$ 25 μm. The total PCB thickness equals 2.972 mm $\pm$ 10%. The antenna has been then characterized using the CEA-Leti far-field facility. The measured gain frequency response (Meas.) is also represented in Fig. 5(b). A peak gain of 27.1 and 29.9 dBi has been obtained at 19.8 and 28.2 GHz, respectively. As presented in this figure, an excellent agreement with the theoretical simulations has been obtained with an absolute error lower than 0.5 dB in both frequency ranges. The ripple in the measured frequency response is probably due to the impact of the mechanical setup used to fix the antenna system in the anechoic chamber, which can introduce interferences produced by spurious reflections. We exclude a possible mismatching of the unit-cell following fabrication errors because, as presented in [25], the simulated reflection coefficient is lower than -14 dB on both frequency bands.

As a summary, the main characteristics and experimental results of the fabricated transmitarray are presented in Table 1 and compared to the actual state-of-the-art on dual-band transmitarray at K/Ka-bands. Note that in Table 1, we present only prototypes where the ratio between down- and up-link bands is particularly challenging, i.e. $\sim$0.65 (19 GHz over 29 GHz). Compared to previous demonstrations with a stacked unit-cell architecture [22], [26], the proposed transmitarray is able to radiate two wideband beams with two orthogonal linear polarizations by using a reduced number of dielectric and metal layers. Despite the 1-bit phase resolution which produces a directivity loss if compared to the case of the continuous phase compensation, an antenna efficiency (i.e. ratio measured antenna gain over directivity) of 72.6 and 71.8%, corresponding to an aperture efficiency (i.e. ratio measured antenna gain over directivity of the uniformly excited in amplitude and phase equivalent aperture ($4\pi \cdot S/\lambda^2$, where S is the square surface of the transmitarray aperture) of 26.1 and 22.3%, has been also demonstrated at DL and UL, respectively. In terms of -3 dB gain bandwidth, the achieved results are at the best level in the literature [23], [24].

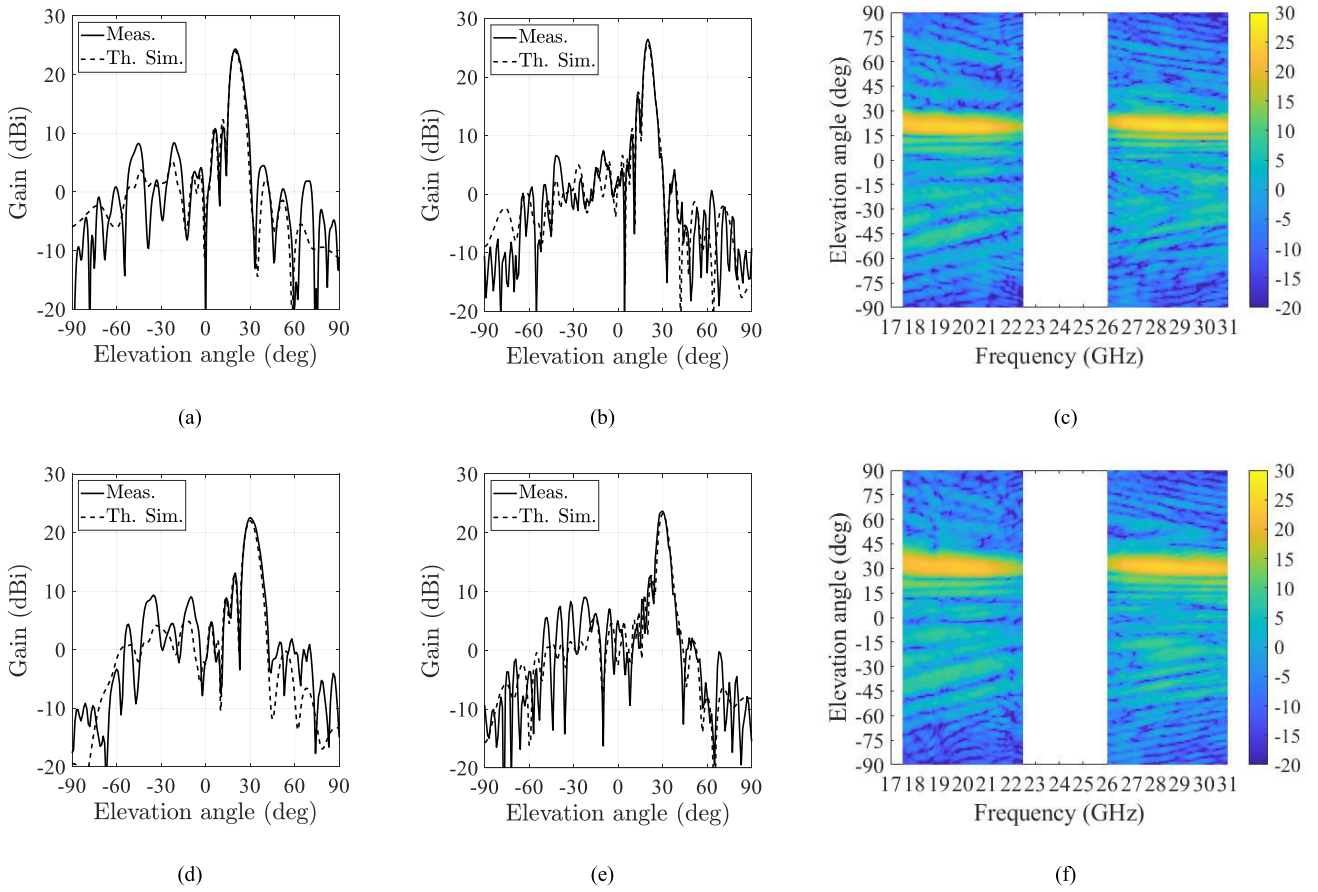

FIGURE 8. Measured and theoretical gain radiation patterns (co-polar) for different beam-pointing directions. (a,b,c) Beam pointing at 20° in H-plane at 19 GHz (a) , 29 GHz (b), and (c) 2D pattern as a function of frequency. (d,e,f) Beam pointing at 30° in H-plane at 19 GHz (d), 29 GHz (e), and (f) 2D pattern as a function of frequency.

As a result, the proposed dual-band dual linearly-polarized antenna has the advantages of a compact aperture, wideband and good efficiency.

The radiation patterns measured at broadside in co- and cross-polarizations in E- and H-planes are presented in Fig. 6 at 19 and 29 GHz. An excellent agreement is demonstrated between experimental and numerical results (array theory and full-wave). The measured cross-polarization discrimination (XPD) at broadside is equal to 33.4 and 37.1 dB at 19 and 29 GHz, respectively. To demonstrate the wideband behavior of the proposed system, the measured gain radiation patterns (E-plane) are plotted in Fig. 7.

B. BEAM-SCANNING PERFORMANCE

To demonstrate the relevance of the proposed transmitarray architecture with respect to SatCom vehicular applications, mechanical steering has been tested by opportunely moving the focal source system along the *y*-axis (corresponding to the H- or E-plane for the DL and UL, respectively) of the flat lens. The movement has been achieved manually to emulate the electromechanical drive which can be used in real system implementations. To generate a beam at 20° and 30°, the focal system is moved in two positions with a distance from the center of 4.6 mm and 6.7 mm, respectively.

The mechanical beam scanning technology is selected here as an alternative mature, robust, and low cost solution to electronically-beam-scanning based transmitarrays. If compared with scanning solutions based on p-i-n diodes [16], [35] or varactors, the use of a fully passive phase-shift surface can be compatible (no non-linear effects) with the high radiated power (>45 dBm at the feed level) required to achieve the adequate EIRP (Effective Isotropic Radiated Power) for LEO satellite connectivity even whit a relatively small antenna aperture. Furthermore, as presented in recent publications [6], [7], the mechanical beam scanning can be also provided considering Risley prisms, which can improve the scanning range of the transmitarray and the total profile.

For brevity purposes, the radiation characteristics are provided only for two main beam directions in H-plane (20° and 30°). The measured and theoretical gain radiation patterns computed at 19 and 29 GHz are presented in Fig. 8 together with the measured 2D patterns as a function of frequency. The scan loss at 19 GHz equals 1.5 dB and 3.4 dB when the antenna beam points at 20° or 30°, respectively. Maximum scan loss of 6 dB is measured at 29 GHz when the beam is steered at 30°. The difference in the scan loss between DL and UL is due to the different periodicity of the unit cell at the two bands. The achieved results are in line with

the actual literature, where mechanical-scanning capabilities up to 45° have been demonstrated [21], [23]. Furthermore, as demonstrated in [34], the scan loss could be mitigated if specific multi-focal phase distributions are applied [34].

IV. CONCLUSION

This paper demonstrates experimentally a wideband, high gain, dual-band, dual linearly polarized, and compact aperture transmitarray for vehicular SatCom applications at K/Ka-bands. A stacked unit-cell architecture has been designed to have a periodicity lower than half of a wavelength at both UL and DL frequency bands. A prototype has been fully characterized to validate the radiation performance at broadside and in scanning when moving the focal point. The experimental results are in very good agreement with the numerical model and prove wideband behavior up to 19.8% with an aperture efficiency $> 20\%$. The proposed antenna can achieve high-gain and beam-steering with a relatively compact surface.

The proposed linearly-polarized transmitarray can be combined with a linear-to-circular polarization converter [36] to generate a dual circular polarization and improve the link budget between the terminal and the satellite. Circularly-polarized patches [27] can be also used on the transmitting layer by opportunely controlling the mutual coupling between the radiating elements operating in the two frequency bands.

REFERENCES

[1] J. Wang, V. Manohar, and Y. Rahmat-Samii, "Enabling the Internet of Things with CubeSats: A review of representative beamsteerable antenna concepts," *IEEE Antennas Propag. Mag.*, vol. 63, no. 6, pp. 14–28, Dec. 2021.

[2] O. Kodheli, E. Lagunas, N. Maturo, S. K. Sharma, B. Shankar, J. F. M. Montoya, J. C. M. Duncan, D. Spano, S. Chatzinotas, S. Kisseleff, J. Querol, L. Lei, T. X. Vu, and G. Goussetis, "Satellite communications in the new space era: A survey and future challenges," *IEEE Commun. Surveys Tuts.*, vol. 23, no. 1, pp. 70–109, 1st Quart., 2021.

[3] R. Correia, T. Varum, J. N. Matos, A. Oliveira, and N. B. Carvalho, "User terminal segments for low-earth orbit satellte constellations," *IEEE Microw. Mag.*, vol. 23, no. 10, pp. 27–58, Oct. 2022.

[4] W. W. Milroy, "Continuous transverse stub element devices and methods of making same," U.S. Patent 5 266 961A, Nov. 30, 1993.

[5] M. Ettorre, F. F. Manzillo, M. Casaletti, R. Sauleau, L. L. Coq, and N. Capet, "Continuous transverse stub array for Ka-band applications," *IEEE Trans. Antennas Propag.*, vol. 63, no. 11, pp. 4792–4800, Nov. 2015.

[6] Z. Zhang, Y. C. Zhong, H. Luyen, J. H. Booske, and N. Behdad, "A low-profile, Risley-prism-based, beam-steerable antenna employing a single flat prism," *IEEE Trans. Antennas Propag.*, vol. 70, no. 8, pp. 6646–6658, Aug. 2022.

[7] H. Lei, Y. C. Zhong, Y. Jia, J. Zhu, Z. Liu, Y. Chen, and Y. Liu, "A low-profile Risley-prism-based 2-D beam-scanning circularly polarized folded transmitarray antenna at Ku-band," *IEEE Trans. Antennas Propag.*, vol. 71, no. 7, pp. 6173–6178, Jul. 2023.

[8] M. U. Afzal, K. P. Esselle, and M. N. Y. Koli, "A beam-steering solution with highly transmitting hybrid metasurfaces and circularly polarized high-gain radial-line slot array antennas," *IEEE Trans. Antennas Propag.*, vol. 70, no. 1, pp. 365–377, Jan. 2022.

[9] K. K. W. Low, T. Kanar, S. Zihir, and G. M. Rebeiz, "A 17.7–20.2-GHz 1024-element K-band SATCOM phased-array receiver with 8.1-dB/K G/T, ±70° beam scanning, and high transmit isolation," *IEEE Trans. Microw. Theory Techn.*, vol. 70, no. 3, pp. 1769–1778, Mar. 2022.

[10] K. K. W. Low, S. Zihir, T. Kanar, and G. M. Rebeiz, "A 27–31-GHz 1024-element Ka-band SATCOM phased-array transmitter with 49.5-dBW peak EIRP, 1-dB AR, and ±70° beam scanning," *IEEE Trans. Microw. Theory Techn.*, vol. 70, no. 3, pp. 1757–1768, Mar. 2022.

[11] J. R. Reis, M. Vala, and R. F. S. Caldeirinha, "Review paper on transmitarray antennas," *IEEE Access*, vol. 7, pp. 94171–94188, 2019.

[12] J. G. Nicholls and S. V. Hum, "Full-space electronic beam-steering transmitarray with integrated leaky-wave feed," *IEEE Trans. Antennas Propag.*, vol. 64, no. 8, pp. 3410–3422, Aug. 2016.

[13] C.-C. Cheng, B. Lakshminarayanan, and A. Abbaspour-Tamijani, "A programmable lens-array antenna with monolithically integrated MEMS switches," *IEEE Trans. Microw. Theory Techn.*, vol. 57, no. 8, pp. 1874–1884, Aug. 2009.

[14] A. Clemente, L. Dussopt, R. Sauleau, P. Potier, and P. Pouliguen, "Wideband 400-element electronically reconfigurable transmitarray in X band," *IEEE Trans. Antennas Propag.*, vol. 61, no. 10, pp. 5017–5027, Oct. 2013.

[15] L. Di Palma, A. Clemente, L. Dussopt, R. Sauleau, P. Potier, and P. Pouliguen, "Circularly-polarized reconfigurable transmitarray in Ka-band with beam scanning and polarization switching capabilities," *IEEE Trans. Antennas Propag.*, vol. 65, no. 2, pp. 529–540, Feb. 2017.

[16] F. F. Manzillo, M. Smierzchalski, J. Reverdy, and A. Clemente, "A Ka-band beam-steering transmitarray achieving dual-circular polarization," in *Proc. 15th Eur. Conf. Antennas Propag. (EuCAP)*, Dusseldorf, Germany, Mar. 2021, pp. 1–4.

[17] A. Aziz, F. Yang, S. Xu, M. Li, and H. Chen, "A high-gain dual-band and dual-polarized transmitarray using novel loop elements," *IEEE Antennas Wireless Propag. Lett.*, vol. 18, no. 6, pp. 1213–1217, Jun. 2019.

[18] R. Y. Wu, Y. B. Li, W. Wu, C. B. Shi, and T. J. Cui, "High-gain dual-band transmitarray," *IEEE Trans. Antennas Propag.*, vol. 65, no. 7, pp. 3481–3488, Jul. 2017.

[19] Y. Cai, K. Li, W. Li, S. Gao, Y. Yin, L. Zhao, and W. Hu, "Dual-band circularly polarized transmitarray with single linearly polarized feed," *IEEE Trans. Antennas Propag.*, vol. 68, no. 6, pp. 5015–5020, Jun. 2020.

[20] S. Yang, Z. Yan, X. Li, and M. Cai, "Dual-band dual-polarized transmitarray with independent control of polarization at each band," *Int. J. RF Microw. Comput.-Aided Eng.*, vol. 32, no. 2, Feb. 2022, Art. no. e22957.

[21] H. Lei, Y. Liu, Y. Jia, Z. Yue, and X. Wang, "A low-profile dual-band dual-circularly polarized folded transmitarray antenna with independent beam control," *IEEE Trans. Antennas Propag.*, vol. 70, no. 5, pp. 3852–3857, May 2022.

[22] S. A. Matos, E. B. Lima, J. S. Silva, J. R. Costa, C. A. Fernandes, N. J. G. Fonseca, and J. R. Mosig, "High gain dual-band beam-steering transmit array for SATCOM terminals at Ka-band," *IEEE Trans. Antennas Propag.*, vol. 65, no. 7, pp. 3528–3539, Jul. 2017.

[23] K. T. Pham, R. Sauleau, E. Fourn, F. Diaby, A. Clemente, and L. Dussopt, "Dual-band transmitarrays with dual-linear polarization at Ka-band," *IEEE Trans. Antennas Propag.*, vol. 65, no. 12, pp. 7009–7018, Dec. 2017.

[24] H. Hasani, J. S. Silva, S. Capdevila, M. García-Vigueras, and J. R. Mosig, "Dual-band circularly polarized transmitarray antenna for satellite communications at (20, 30) GHz," *IEEE Trans. Antennas Propag.*, vol. 67, no. 8, pp. 5325–5333, Aug. 2019.

[25] R. Madi, A. Clemente, and R. Sauleau, "Dual-band dual-linearly polarized transmitarray at Ka-band," in *Proc. 50th Eur. Microw. Conf. (EuMC)*, Jan. 2021, pp. 340–343.

[26] X. Tong, Z. H. Jiang, Y. Li, F. Wu, J. Wu, R. Sauleau, and W. Hong, "An integrated dual-band dual-circularly-polarized shared-aperture transmit-array antenna for K-/Ka-band applications enabled by polarization twisting elements," *IEEE Trans. Antennas Propag.*, vol. 71, no. 6, pp. 4955–4966, Jun. 2023.

[27] F. Diaby, A. Clemente, K. T. Pham, R. Sauleau, and L. Dussopt, "Circularly polarized transmitarray antennas at Ka-band," *IEEE Antennas Wireless Propag. Lett.*, vol. 17, no. 7, pp. 1204–1208, Jul. 2018.

[28] R. Madi, A. Clemente, and R. Sauleau, "Dual-band, dual-linearly polarized transmitarrays for SATCOM applications at Ka-band," in *Proc. 16th Eur. Conf. Antennas Propag. (EuCAP)*, Madrid, Spain, Mar. 2022, pp. 1–4.

[29] S. Maci, G. Biffi Gentili, P. Piazzesi, and C. Salvador, "Dual-band slot-loaded patch antenna," *IEE Proc.-Microw., Antennas Propag.*, vol. 142, no. 3, pp. 225–232, 1995.

[30] A. Clemente, L. Dussopt, R. Sauleau, P. Potier, and P. Pouliguen, "1-bit reconfigurable unit-cell based on PIN diodes for transmit-array application in X-band," *IEEE Trans. Antennas Propag.*, vol. 60, no. 5, pp. 2260–2269, May 2012.

[31] A. Clemente, L. Dussopt, R. Sauleau, P. Potier, and P. Pouliguen, "Focal distance reduction of transmit-array antennas using multiple feeds," *IEEE Antennas Wireless Propag. Lett.*, vol. 11, pp. 1311–1314, 2012.
[32] H. Kaouach, L. Dussopt, J. Lanteri, T. Koleck, and R. Sauleau, "Wideband low-loss linear and circular polarization transmit-arrays in V-band," *IEEE Trans. Antennas Propag.*, vol. 59, no. 7, pp. 2513–2523, Jul. 2011.
[33] P. Zhang, X. Zhu, X. Shu, C. Zhao, Z. Tao, P. Chu, and M. Jiang, "A 20/30 GHz dualband dual circularly polarized antenna hybridizing folded refelctarray and folded transmitarray," in *IEEE MTT-S Int. Microw. Symp. Dig.*, vol. 1, Harbin, China, Aug. 2022, pp. 1–3.
[34] T. K. Pham, L. Guang, D. González-Ovejero, and R. Sauleau, "Dual-band transmitarray with low scan loss for SATCOM applications," *IEEE Trans. Antennas Propag.*, vol. 69, no. 3, pp. 1775–1780, Mar. 2021.
[35] A. Clemente, R. Madi, F. F. Manzillo, M. Smierzchalski, J. Reverdy, and R. Sauleau, "Reconfigurable transmitarrays at Ka-band with beam-forming and polarization agility," in *Proc. 17th Eur. Conf. Antennas Propag. (EuCAP)*, Mar. 2023, pp. 26–31.
[36] K. T. Pham, A. Clemente, D. Blanco, and R. Sauleau, "Dual-circularly polarized high-gain transmitarray antennas at Ka-band," *IEEE Trans. Antennas Propag.*, vol. 68, no. 10, pp. 7223–7227, Oct. 2020.

REDA MADI received the B.S. and M.S. degrees in electronics and telecommunications from the University of Rennes 1, France, in 2016 and 2018, respectively, where he is currently pursuing the Ph.D. degree in electronics and telecommunication systems. His master's thesis project was developed at the Canon Research Centre France, Cesson-Sévigné, France, where he worked on the development of plastic lens components at millimeter wave frequencies. From 2019 to 2022, he was a Research Assistant at CEA-Leti, Grenoble, France, where he worked on his Ph.D. project. Since 2022, he has been an System Engineer at Capgemini, Blagnac, France, and at OneWeb, Toulouse, France. His research interests include antenna solutions for SatCom systems and electronically reconfigurable electromagnetic surfaces.

ANTONIO CLEMENTE (Senior Member, IEEE) received the B.S. and M.S. degrees in telecommunication engineering and remote sensing systems from the University of Siena, Italy, in 2006 and 2009, respectively, the Ph.D. degree in signal processing and telecommunications, and the Habilitation à Diriger des Recherches degree from the University of Rennes 1, France, in 2012 and 2021, respectively. His master's thesis project was developed at the Technical University of Denmark (DTU), Lyngby, Denmark. From 2009 to 2012, he was a Research Assistant at CEA-Leti, Grenoble, France. In 2012, he joined the Research and Development Laboratory, Satimo Industries, Villebon-sur-Yvette, France. Since 2013, he has been a Research Scientist at CEA-Leti. From 2016 to 2018, he was the Technical Coordinator of the H2020 Joint Europe and South Korea 5G-CHAMPION Project. Since 2018, he has been responsible for the antenna activity for wireless backhauling and GNSS applications in the joint laboratory between CEA-Leti and Radiall, France. He has authored or coauthored more than 145 papers in international journals and conferences and received 21 patents. He has been involved in more than 30 research projects at the national and international levels. His current research interests include electronically reconfigurable transmitarray antennas, millimeter-wave and sub-terahertz antenna-in-package (AiP), periodic or quasiperiodic structures and electromagnetic surfaces up to sub-THz frequencies, near-field focused systems, antenna theory, fundamental limitations, and synthesis, and near- and far-field antenna measurements. He received the Young Scientist Award from the 2012 International Symposium of Antenna Technology and Applied Electromagnetics (ANTEM) and the Best Antenna Design and Applications Paper Award from the 2019 European Conference on Antennas and Propagation (EuCAP). He was a co-recipient of the Young Engineer Prize at EuMC 2021, the Best Paper Award at JNM 2015 (19emes Journées Nationales Microondes), and the 2019 ETRI Journal Best Paper Award. In 2019, he was a Finalist for the "Microwave Prize" at the EuMC 2019. He serves as a reviewer for numerous journals in the field of microwave, antennas, and propagation.

RONAN SAULEAU (Fellow, IEEE) received the master's and M.Sc. degrees in electrical engineering and radio communications from the Institut National des Sciences Appliquées, Rennes, France, in 1995, the Agrégation degree from the Ecole Normale Supérieure de Cachan, France, in 1996, and the Ph.D. degree in signal processing and telecommunications and the Habilitation à Diriger des Recherches degree from the University of Rennes 1, Rennes, France, in 1999 and 2005, respectively.

He was an Assistant Professor and an Associate Professor at the University of Rennes 1, from September 2000 to November 2005, and from December 2005 to October 2009, respectively. He has been a Full Professor with the University of Rennes 1, since November 2009. He was the Co-Director with the Department of Antenna and Microwave Devices, IETR, and the Deputy Director at IETR, from 2012 to 2016. He is now the Director at IETR. His research interests include numerical modeling, millimeter-wave beam steering antennas, substrate integrated waveguide antennas, lens-based focusing devices, periodic and non-periodic structures (FSS, metasurfaces, polarizers, reflectarrays, and transmitarrays), and biological effects of millimeter waves. He has been involved in more than 70 research projects at the national and European levels and has co-supervised 27 post-doctoral fellows, 57 Ph.D. students, and 50 master's students. He has received 20 patents and is the author or coauthor of more than 280 journal articles and 580 publications in international conferences and workshops. He received the 2004 ISAP Conference Young Researcher Scientist Fellowship, Japan, and the First Young Researcher Prize in Brittany, France, in 2001, for his research work on gain-enhanced Fabry-Perot antennas. In September 2007, he was elected as a Junior Member of the "Institut Universitaire de France." He was awarded the Bronze Medal by CNRS, in 2008, and the Silver Medal, in 2020. He also received the 2021 Antenna EurAAP Award. He was a co-recipient of several international conference awards with some of his students (International School of BioEM 2005, BEMS'2006, MRRS'2008, E-MRS'2011, BEMS'2011, IMS'2012, Antem'2012, BioEM'2015, EuCAP'2019, EuCAP'2021, and EuMW'2022). He served as a Guest Editor for IEEE TRANSACTIONS ON ANTENNAS AND PROPAGATION Special Issue on "Antennas and Propagation at mm and sub mm Waves." He served as a national delegate for several EU COST actions. He has served as a national delegate for EurAAP and as a Member of the Board of Director of EurAAP, from 2013 to 2018.